European Journal of Pharmaceutical Sciences 189 (2023) 106537

Contents lists available at ScienceDirect

European Journal of Pharmaceutical Sciences

journal homepage: www.elsevier.com/locate/ejps

Protein corona formation on lipidic nanocapsules: Influence of the interfacial PEG repartition

Vincent Lebreton [a,b,*], Samuel Legeay [a], Anastasiia Vasylaki [a], Frédéric Lagarce [a,b], Patrick Saulnier [a,b]

[a] MINT, UNIV Angers, SFR-ICAT, INSERM U1066, CNRS 6021, Angers 4208, France
[b] CHU Angers, Angers 49033, France

ARTICLE INFO

Keywords:
Corona formation
Lipid nanocapsules
Plasmatic media
Electrokinetic
Physicochemical properties

ABSTRACT

The parameters currently used for characterization of nanoparticles, such as size and zeta potential, were not able to reflect the performance of a nanocarrier in the biological environment. Therefore, more thorough *in vitro* characterization is required to predict their behavior *in vivo,* where nanoparticles acquire a new biological identity due to interactions with biomolecules. In this present study, we performed *in vitro* characterization in biological fluids for lipid nanocapsules (LNCs) with varying means sizes (50 nm and 100 nm), different electrical surface charges and different Poly Ethylene Glycol (PEG) compositions. Then, different methods were applied to show the impact of the protein corona formation on LNCs. Even if all formulations attached to plasmatic proteins, a higher thickness of corona and highest protein binding was observed for certain LNC50 formulations. A better knowledge of the phenomenon of protein adsorption over NPs in the plasmatic media is a cornerstone of clinical translation. In fact, after short blood circulation time, it is not the initially designed nanoparticle but the complex nanoparticle bearing its protein corona which circulates to reach its target.

1. Introduction

Organic or inorganic nanoparticles (NPs) have been used for the last few decades to improve drug delivery (Tran et al., 2017; Park et al., 2022). However, if some successful medical applications have been implemented in the domain of cancer therapy or more recently in infectious diseases with SARS-COV-2 vaccines (Nanomedicine, 2020; Machhi et al., 2021), there is a need for a better knowledge about NP interactions with biological fluids (Lynch and Dawson, 2008). A basic understanding of the link between physicochemical properties of NPs and the impact on protein adsorption seem essential in order to improve the design and development of well-characterised NPs for the future (Sharifi et al., 2020; Bertrand et al., 2017). NPs are immediately surrounded by proteins after contact with biological fluids and eventually change their synthetic identity to a new biological one (Caracciolo, 2015; Pareek et al., 2018). Interactions between NPs and proteins have been described since the 70 s, Tyrell et al. found for the first time albumin, alpha- and beta-globulin interaction with liposomes and studied the effect on this interaction on their uptake by cells (Tyrrell et al., 1977). The intensive study of the consequences of this aggregation phenomenon has started around 2007, when Dawson *et al.* described protein coating and gave it the name of "protein corona" (Lynch and Dawson, 2008; Cedervall et al., 2007; Lundqvist et al., 2008). Nowadays, it was widely recognised that NPs and biomolecules establish different interactions, were several factors are known to affect the protein corona composition, which includes morphological and chemical NP characteristics (Caracciolo, 2015; Palchetti et al., 2016; Park, 2020; Ke et al., 2017). The protein corona is complex and variable because biological fluids such as plasma contain as many as 3700 proteins (Lynch and Dawson, 2008; Cedervall et al., 2007; Lynch et al., 2007) and it has been estimated that approximately 50 to 150 proteins can interact with NPs (Tenzer et al., 2011; Treuel et al., 2015). In a general pattern, corona is constituted by a "hard-corona" based on strong NP/proteins links and a "soft corona" resulting from weak binding, allowing dynamic protein exchanges on the NP surface (Kristensen et al., 2019; Vilanova et al., 2016; Kari et al., 2020). In addition some components of the protein corona called opsonins enhance uptake by the specialised cells of the reticuloendothelial system (RES) leading to an increased and faster elimination (Fang et al., 2019; Gustafson et al., 2015; Mcgoron et al., 2019). Understanding this phenomenon is an important milestone of the

* Corresponding author at: IRIS1 – IBS – CHU, 4 rue Larrey, MINT Inserm U1066, CNRS 6021, Angers 49100, France.
E-mail address: vincent.lebreton@univ-angers.fr (V. Lebreton).

https://doi.org/10.1016/j.ejps.2023.106537
Received 17 April 2023; Received in revised form 4 July 2023; Accepted 22 July 2023
Available online 23 July 2023

NP's development because the entire impact of the protein corona on the fate of NPs and thus on drug delivery patterns remains partially unknown. Indeed, if there are a lot of data concerning inorganic NPs, studies on soft particles remain poor concerning protein corona especially on Lipid Nanocapsules (LNCs) such as those that have been developed by our team since 2000 (Heurtault et al., 2002). These nanocapsules have been used to encapsulate many molecules in their lipid core (Peltier et al., 2006; Roger et al., 2011; Morille et al., 2010; Saliou et al., 2013). Among the huge number of organic NPs, the main advantage of LNCs lies in their formulation with modifying their composition only (water/oil ratio, surfactant concentrations), their formulation enables a good control of their physico-chemical characteristics mainly the surface characteristics (Mouzouvi et al., 2017; Perrier et al., 2010; Hirsjärvi et al., 2013; Huynh et al., 2009). This is why it is particularly relevant to study the influence of the size, the surface charge and the interfacial properties on protein coating in the case of LNCs to obtain optimised formulations. On previous studies which were conducted by our team, Groo et al., have demonstred that post-inserting PEG to LNCs enables an increase of the blood circulation time of paclitaxel b (Groo et al., 2015). Nevertheless, we recenty published a study about LNCs with pre-mixing PEG which on the onse side highlights an increase time of blood circulation of LNCs 85 nm, but on the other side a sharp decrease blood time residence of LNCs 50 nm (Lebreton et al., 2022). The aim of the present work is to demonstrate how protein corona can modify the synthetic identity of LNCs for different protein corona by using different pegylated surfactants at the first steps of the LNC formulation. In this paper, we offer an analysis of the effects of LNCs (different sizes and different interfacial molecular conformation) on the protein corona formation by using the soft particles analysis described by Ohshima. This electrokinetic method is able to quantify the electrical charge density in the accessible ionic layer inside the LNCs shell (Ohshima, 2009; Ohshima, 2006).

2. Materials and methods

2.1. Materials

Dulbecco's Phosphate Buffered Saline (PBS), octadecylamine (stearylamine), Bovine Serum Albumin (BSA), sodium chloride and potassium chloride were supplied by Sigma-Aldrich (Saint-Quentin-Fallavier, France). Kolliphor® HS-15 (PEG 660 and polyethylene glycol 660 hydroxystearate mixture) was purchased from BASF (Ludwigshafen, Germany). Lipoid® S75–3 (phosphatidylcholine and phosphatidylethanolamine mixture) were purchased from Lipoid GmbH (Steinhausen, Switzerland). Captex® 8000 (glyceryl tricaprylate) was kindly provided by Abitec Corporation (Columbus, OH, USA). DSPE-mPEG-2000 (1,2-distearoyl-sn-glycero-3-phosphoethanolamine-N-[methoxy(polyethylene glycol)−2000] (ammonium salt)) was purchased Avanti Polar Lipids (Alabaster, AL, USA). Ultrapure water was obtained from a Milli-Q® Advantage A10 System (Merck Millipore, Darmstadt, Germany). Fetal Bovine serum (FBS) was purchased from Biowest (Nuaillé, France).

Fresh rat plasma was obtained directly after intracardiac blood puncture on Sprague Dawley male rat (Janvier labs, Saint-Genis-Laval, France) on EDTA K2 tube (BD Vacutainer®, Franklin Lakes, USA).

2.2. Formulation of lipid nanocapsules (LNCs)

LNCs were formulated using a phase inversion process that was previously established (Heurtault et al., 2002). For the different formulations, the compounds were precisely weighed as mentioned in the supplementary Table S1. For positively and negatively charged LNCs, 1.4 mg of stearylamine (SA) or 7.0 mg of DSPE-mPEG-2000 (PEG) were added, respectively in the starting premix with all other compounds. The mixture was briefly stirred at 200 rpm agitation speed at room temperature to obtain an oil/water emulsion. Then, four cycles of heated and cooled phases from 60 to 90 °C were performed to detect the inverted phase close to 70 °C. On the last run, of this inversion phase, LNCs were formed after quenching with 625 mg of cold water and stirring for 30 min. LNC suspensions were filtered through a 0.22 μm filter before use. Were finally obtained, six formulations of LNCs with two sizes: 50 nm (LNC-50) and 100 nm (LNC-100), surface modifications: DSPE-mPEG-2000 (PEG) (LNC-50-PEG; LNC-100-PEG) and stearylamine (SA) (LNC-50-SA; LNC-100-SA).

2.3. Size and zeta potential: Measurements before and after incubation

All nanoparticles were characterised in terms of size, and zeta potential (ZP) using a Malvern Zetasizer Nano ZS setup (Malvern Panalytical, Worcestershire, UK). Size was determined by a dynamic light scattering method with a 173° backscattering detection measurement angle, after 3 measurements, each constituting at least 10 runs. Each measurement was performed in triplicate at 25 °C. A 1:100 dilution of nanoparticle suspension in ultrapure water was achieved in order to ensure a convenient scattering intensity on the detector. On similar conditions of dilution, ZP was also estimated by 3 measurements with automatic selection of the number of runs (from 10 to 100) through determination of the electrophoretic mobility in a folded capillary cell and after applying the Smoluchowski equation.. Were briefly diluted LNCs suspensions in ultrapure water by a factor ranging from 5×10^5 to 1×10^6 and then slowly injected into the sample chamber using a 1 mL syringe pump with ta flow rate of 3–4 μL per second. The video sequences of the nanoparticles were captured over 60 s (5 replicates) and then analysed by the NTA analytical software version 3.2. Finally, NTA provided the particle distribution width parameters, which was calculated following the equation: Span = (D90 − D10)/D50 where D10, D50, and D90 represent the diameter (nm) at the 10th, 50th (median), and 90th percentiles of the distribution histogram, respectively. All experiments were carried out at 25 °C and similar conductivity values. After incubation in FBS or rat plasma, the average hydrodynamic diameter and polydispersity index of LNCs were measured using the same method as the initial measurement but without the dilution before analysis to avoid modifications of the protein corona around LNCs. In the same conditions, ZP was determined after 3 measurements of each sample without dilution., the conductivity of each sample was measured to enable a suitable comparison between ZP.

2.4. Incubation with proteins to study the protein corona formation

2.4.1. Fetal bovine serum (FBS)

As a first step, in order to study the evolution of ZP and size after protein contact, it was decided to perform the experimentation with LNC 50 nm. LNCs 50 nm were incubated with different proportions (v:v) of FBS medium equivalent to 0 to 16 g/L of BSA with a final fixed solution of LNCs suspension (1:100) (supplementary on Table S2). To keep similar conductivity, PBS dilution medium was considered as the best choice. All mix combinations were performed on Ultra High Recovery Microcentrifuge Tubes (STARLAB International GmbH, Hamburg, Germany) to minimize protein binding to the plastic surface. The LNCs were incubated for 1 h at 37 °C in lab oven (Memmert, Schwabach, Germany).

2.4.2. Rat plasma

In order to assess protein-corona formation, the second step consisted in the incubation of the six different LNC formulations with fresh rat plasma for 1 h at 37 °C in the previously described conditions. For plasma preparation, EDTA was chosen as an appropriate anticoagulant since it does not alter the protein corona composition (Berrecoso et al., 2020; Lundqvist et al., 2017). In order to make accurate comparisons between the six formulations, the ratio of nanoparticles surface area to the volume of plasma was established thanks to *in vivo* relevant LNCs plasma-particle concentrations. After intravenous injections of each LNC suspension (fixed dose 2.10^{14} part/ 100 g of rat), the initial concentrations (C_{init}) were close to 5.0×10^{13} part/mL (Lebreton et al., 2022). As

the surface area of LNC 50 nm (A_{LNC50}) was considered as the reference, the surface area (Eq. (2)) of the formulation was calculated and the result for one particle (7850 nm^2) was considered as the target. Then, to estimate the surface area of the formulation in blood compartment after injection, A_{LNC50} was multiplied by the C_{init} to obtain the required standardised surface area, 3.925×10^{17} nm^2/ml for each experimentation.

The volume of LNC suspension added to plasma was calculated for each formulation according to the following formula:

$$V_{LNC} = \frac{3.925 \times 10^{17}}{A_{LNC} \times C_{LNC}} \quad (1)$$

where A_{LNC} is the surface area of a LNC (in nm^2), and C_{LNC} is the concentration of LNC (in particles/ml). Since LNC have a spherical shape, A_{LNC} was calculated as follows:

$$A_{LNC} = 4\pi r^2 \quad (2)$$

After incubation, nanoparticle size and ZP were measured using the Zetasizer Nano and compared to the initial parameters of the formulation.

2.5. Isolation of LNCs-Corona and free proteins with size exclusion chromatography

In order to separate LNCs bearing protein corona from free proteins present in plasma, size exclusion chromatography (SEC) was performed using Waters 600 HPLC system (Waters, Saint-Quentin-en-Yvelines, France) equipped with protein KW-803 column (Shodex, New York, NY, USA) (Gazaille et al., 2021). Detection was performed using a UV (λ = 280 nm) and a refractive index detector. PBS was used as a mobile phase at a flow rate of 0.75 mL/min, sample injection volume constituted 100 µL. Chromatographic profiles were obtained for rat plasma, LNCs formulations, and mixtures of LNC with plasma incubated during 1 h at 37 °C.

2.6. Protein quantification of corona with micro bicinchoninic acid (micro-BCA) assay

The micro-BCA assay was used to quantify the amount of protein absorbed onto the LNC surface after incubation in plasma. The assay was performed using the Thermo Scientific™ Micro BCA™ Protein Assay Kit (Thermo Fisher Scientific, Rockford, IL, USA) according to the manufacturer's instructions. Were briefly mixed, 150 µL of protein-containing samples with 150 µL of working reagent in a microplate well, incubated at 37 °C for 2 h, and the absorbance was measured at 562 nm on a SpectraMax M2 microplate reader (Molecular Devices, San Jose, CA, USA). Additionally, a set of protein standards with varying mass concentration of bovine serum albumin between 0 and 200 µg/mL was tested in order to build a standard curve, from which the protein concentration in the samples was estimated. The obtained protein concentration was corrected with dilution factor introduced during SEC and the quantity of coeluted plasma proteins was subtracted. In order to make comparisons between different formulations, the quantity of absorbed protein was expressed as the density of protein on the LNC surface in µg/nm^2.

2.7. Semi qualitative analysis: SDS-PolyAcrylamide gel electrophoresis (PAGE)

The separation step from SEC of interesting harvested fractions and after the protein quantification step with micro-BCA, the aliquots were diluted to reach a maximum of 20 µg of proteins per samples in maximum volume of 40 µL. These samples were treated with a buffer Laemmli (previously mixed with 2-mercaptoethanol) (BioRad, Hercules, California, USA), heated at 100 °C for 5 min. Then, each aliquot was electrophoresed in separated lanes to 4–20% acrylamide denaturing SDS-polyacrylamide gel, a mini-protean® TGX™ precast gel (BioRad, Hercules, California, USA). The first lane was attributed to the molecular weights 10–190 kDa, Precision Plus Protein™ standard (BioRad, Hercules, California, USA), the electrophoresis cell was filled with a buffer Tris-Glycine-SDS (BioRad, Hercules, California, USA), and electrophoresis conditions have been fixed to 100 V for 90 min. After that, the gels were washed with water and stained with Coomassie brilliant blue G-250 (BioRad, Hercules, California, USA) during 30 min and destained in a water acetic acid solution. Finally, the gels were read with gel imager apparatus (Axygen, San Fransisco, California, USA).

2.8. Electrokinetic measurements

In order to determine the pseudo-charge density (ZN) and the accessibility layer to ions or proteins (1/λ), the electrophoretic mobility of LNCs according to Ohshima, who thoroughly described the soft-particle theory (Ohshima, 2009). Thus, it was decided to perform an electrophoretic mobility measurement with NanoZS of our different LNCs formulations (LNC-50, LNC-50-PEG, LNC-100, LNC-100-PEG for different KCl concentrations. The four formulations were diluted into a potassium chloride solution with variable concentrations ranging from 0 to 0.15 mol/L. The average and standard deviation values were estimated from 3 measurements of each sample. Experimental values were fitted by using the following equation:

$$\mu = \frac{\varepsilon_r \varepsilon_0}{\eta} \frac{(\psi_0/\kappa_m) + (1/\lambda)\psi_{DON}}{(1/\kappa_m) + (1/\lambda)} + \frac{\rho_{fix}}{\eta}\left(\frac{1}{\lambda}\right)^2 \quad (3)$$

where ψ_0 is the surface potential and ψ_{DON} is the Donnan potential in the polyelectrolyte layer (Fig. 1).

Both parameters (ψ_0 and ψ_{DON}) are calculated according to Eqs. (4) and (5).

$$\psi_0 = \psi_{DON} + \frac{2n\kappa T}{\rho_{fix}} \left\{ 1 - \left[\left(\frac{\rho_{fix}}{2zne} \right)^2 + 1 \right]^{1/2} \right\} \quad (4)$$

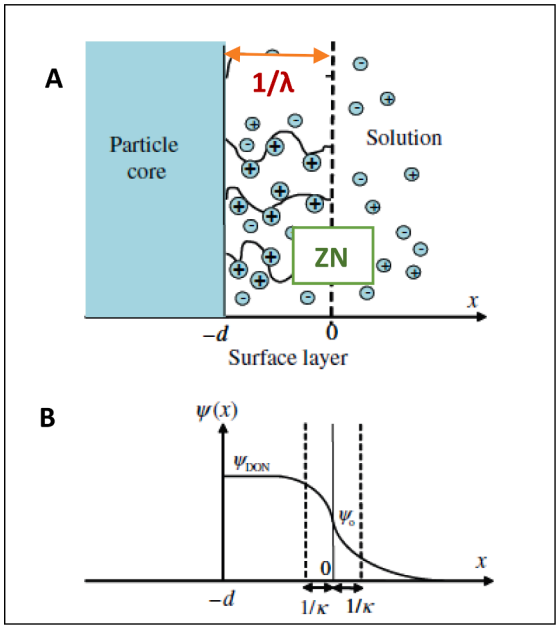

Fig. 1. (A) Schematic representation of ion distribution (upper) with 1/λ (nm) the thickness of ion-penetrable layer and ZN (C/m^3) the pseudo-electrical charge of this accessible layer. (B) Representation of the potential distribution ψ(x) (lower) across an ion-penetrable surface charge layer. (*Adapted from Ohshima* (Ohshima, 2009)).

$$\psi_{DON} = \frac{\kappa T}{ze} \ln\left\{ \frac{\rho_{fix}}{2zn} + \left[\left(\frac{\rho_{fix}}{2zne} \right)^2 + 1 \right]^{1/2} \right\} \quad (5)$$

κ_m is given the following Eq. (6)

$$\kappa_m = \kappa \sqrt[4]{1 + \left(\frac{\rho_{fix}}{2zne} \right)^2} \quad (6)$$

with κ, the Debye length is calculated using

$$\kappa = \sqrt{\frac{\sum_{i=1}^{N} z_i^2 e^2 n_i}{\varepsilon_r \varepsilon_0 \kappa T}} \quad (7)$$

where the physical constants were defined as ε_0: electric permittivity of free space; ε_r: electric permittivity of water; T: temperature; z_i: charge number of ion species *i*; *z*: charge number of electrolytes (supposed to be symmetrical); *e*: elemental charge; κ: Boltzmann's constant; *n*: bulk electrolyte molar concentration; n_i: bulk ion *i* molar concentration; *N*: charge unit molar concentration in the LNC shell. ρ_{fix}: pseudo-charge density in the accessible layer; λ^{-1} : depth of the accessible layer.

On Fig. 1, the particle with a core radius is surrounded by a PEG layer and $1/\lambda$ represents the depth accessible to ions (K^+, Cl^-) Fig. 1A is adapted from Ohshima (Ohshima, 2006). Fig. 1B presents the Donnan potential (ψ_{DON}) in the polyelectrolyte layer and the potential (ψ_0) at the surface.

2.9. Statistical analysis

All data are presented as a mean ± standard deviation, based on the data from experiments performed in triplicates unless stated otherwise. Statistical significance was determined by means of a *t*-test between control and experiment values, or analysis of variance with Tukey test post hoc test, using GraphPad Prism 9.3.0 software (GraphPad Software Inc., La Jolla, CA, USA). Differences were considered statistically significant at $p < 0.05$.

Multiple comparisons for more than two groups were performed by using a one-way analysis of variance (ANOVA) followed by Fisher's test to determine the significance of difference among all paired combinations. p-values lower than 0.05 were considered to be statistically significant.

3. Results and discussion

3.1. Zeta potential and size of LNCs after FBS contact

This work started with a study on classical LNC 50 to understand and check if the methods were available to detect the presence of protein on the different NPs. LNC 50 were formulated with ZP around −4.3 ± 0.2 mV. Because after 1 h of incubation, the size and ZP were stable (data not shown), all the measurements were performed after 1 h of incubation with proteins. After incubation in different FBS solutions (concentrations reported as equivalent BSA concentration), ZP started to decrease and then increased significantly when the concentration of BSA reached 4 g/L (Fig. 2). This phenomenon could be attributed to the saturation of the NPs surface with strong negative charged proteins binding ("hard corona") and then the formation of the "soft corona" with proteins less negatively charged or neutrally charged. A control group without LNCs, containing FBS only, allowed to ensure that the measurement was related to the complex LNC-protein ZP evolution and not to the protein alone.

Adding to that, as shown in Fig. 3, the distribution profile of LNCs with FBS in aqueous solution presented two peaks where the first can be attributed to albumin (the main protein of FBS). Indeed, with regard to the special size measurement of pure BSA solution shown on supplementary data (Fig. S3), a hydrodynamic diameter around 5 nm (PDI <0.3) was measured. In our case, it was previously demonstrated that albumin and NPs can be significantly distinguished in size measurement (Filipe et al., 2010; Gupta and Roy, 2020). Even if there is an important difference of hydrodynamic sizes between albumin (5 nm) and LNC (50 nm), these two elements seem well separated even if the intensity of the scattered light is proportional to the sixth power of the particle diameter making this technique very sensitive to the presence of large particles (Demeester et al., 2005).

In order to obtain more accurate results on corona formation and to evaluate the effect of surface modification of LNC on the protein corona formation, the FBS was replaced by plasma and six different formulations were tested (Berrecoso et al., 2020; Gupta and Roy, 2020).

3.2. Modifications of the protein corona formation following the surface of LNCs after plasma contact

3.2.1. Physical characteristics modifications

Whole plasma was chosen as the most adequate medium for protein corona experiments because media like serum do not include

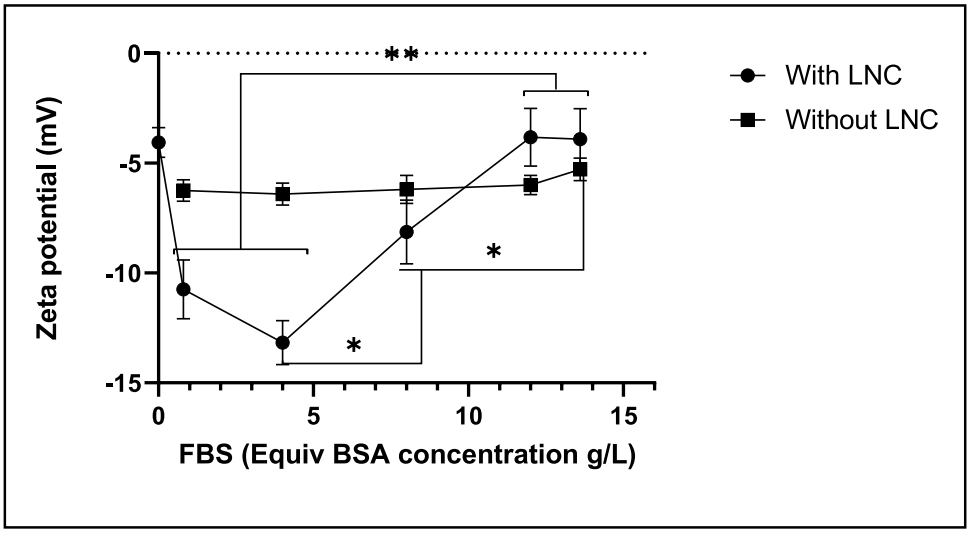

Fig. 2. Zeta potential (mV) evolution of LNC 50 nm after incubation in a solution of Fetal Bovine Serum (FBS) expressed in equivalent bovine serum albumin concentration (g/L). *Paired t-test** p< 0.001; *p<0.05.*

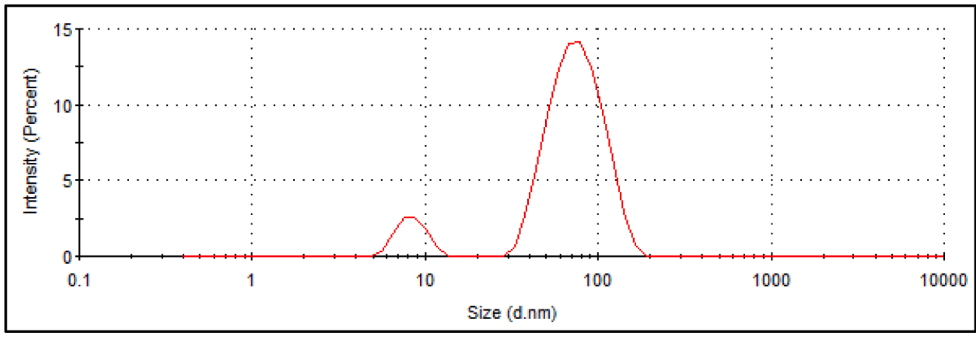

Fig. 3. Distribution of size (nm) LNC 50 nm after with Fetal Bovin Serum (FBS). (*NanoZetaSizer; Malvern Panalytical*).

coagulation proteins that may constitute a part of protein corona (Berrecoso et al., 2020). In Fig. 4A, it was observed that the increase in size after contact with rat plasma proteins was similar among 50 and 100 nm formulations, with the exception of LNC 50 nm PEG (negatively charged) that displayed a larger increase in size. As for the change in ZP (Fig. 4B), regardless of initial surface charge, all the formulations reached a similar value around −5 mV. Similar results have been recently described by Hierro-Oliva et al. where three different titanium inorganic NPs had similar ZP after protein adsorption (Hierro-Oliva et al., 2021). It can be noted that the thickness of protein corona on LNC 50 nm PEG is considerably higher than in other formulations. Using the analysis of variance (ANOVA) method, it was found that particle surface charge has a significant influence on protein corona thickness ($p < 0.05$), while Tukey post hoc test has showed that the difference lies between 50 nm SA and 50 nm PEG formulations. This result concerning LNC-50-PEG seems different than the usual previous results obtained with pegylated NPs where the PEG post-insertion reduced the protein adsorption (Pelaz et al., 2015; Walkey et al., 2012; Gref et al., 2000). Moreover, in previous cited studies such as Pelaz et al. (2015), the additionnal PEG layer was more homogeneous because it was located in the external part of the NP interface after the final step. In our case, the DSPE-mPEG 2000 is mixed at the starting of the formulation with Kolliphor® HS-15 (hydroxystearate of PEG 600). One can suppose an interfacial demixion of both molecules during the formulation leading to inhomogeneous zones at the LNC surface.Thus the conformation of PEG chains at the surface of NPs is modified and different compared to most cases with usual graft pegylation technique (Cieślak et al., 2017, Allen et al., 2002; Mare et al., 2018). Otherwise, this phenomenon would partly explain the increased clearance was observed after intravenous injection on rats (Lebreton et al., 2022).

3.3. Separation of LNC with protein corona from free plasma proteins

Then, the separation of LNC with protein corona from plasma was performed using size exclusion SEC, in order to separate LNC from free proteins and to perform a protein analysis. Firstly, chromatographic profiles for rat plasma and blank LNC formulations were obtained and used as controls. The retention times for these compounds were established. Then, the mixtures of LNC with plasma incubated for 1 h at 37 °C were separated (Fig. 5). Peak of interest, F1 corresponds to the peak that has the same retention time as blank LNC with possible LNC covered by protein corona.

3.4. Quantification and semi-qualitative approach of protein corona surrounding LNCs

After separation, the protein amount bound to each LNC formulation was quantified using a micro BCA protein assay. Since interference of lipids with BCA assay was reported in the literature (Partikel et al., 2019), blank LNC formulations without incubation in plasma were also included in the assay. No contribution was detected from these samples. Fig. 6A demonstrates that the quantity of protein bound to LNC, expressed as the density of protein on the LNC surface in μg/nm^2 is similar for all formulations except LNC 50 nm PEG, which has significantly higher (approximately 3-fold) quantity of protein per unit of the surface area of nanoparticles.

Thus, after the quantification step, we evaluated if the composition of the protein corona formed on LNCs after exposition to rat plasma was also linked to their physicochemical properties. Indeed, following removal of the unbound and loosely bound proteins, the protein constituents of the protein corona were qualitatively analysed by SDS-PAGE performed under reducing conditions (Fig. 6B). The protein profiles were fairly similar, but the intensities of the bands differed. The

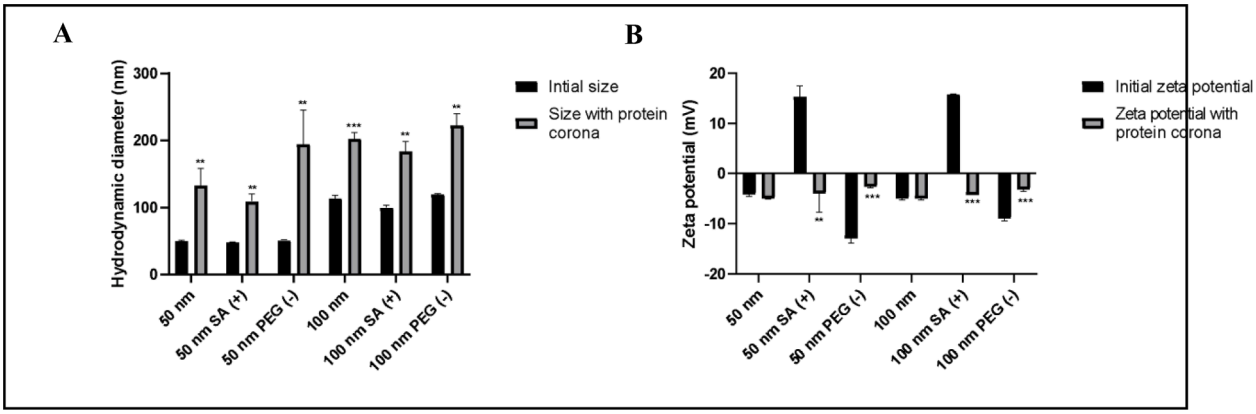

Fig. 4. **(A)** Hydrodynamic diameter (nm) for six different LNCs formulations after 1 h incubation in rat plasma. **(B)** Zeta potential (mV) of six different LNCs formulations after 1 h incubation in rat plasma. *Paired t-test **p < 0.01, *** p < 0.001 compared to initial measurement.*

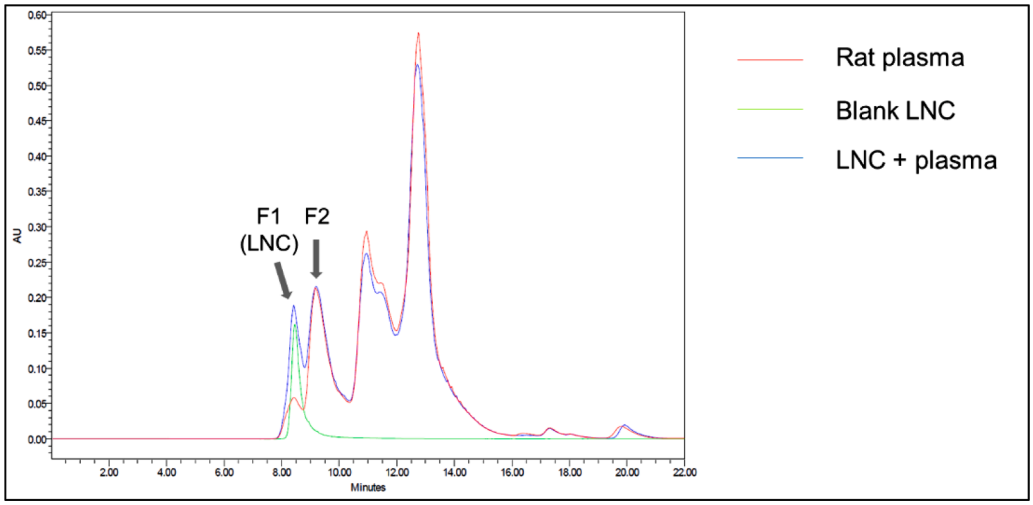

Fig. 5. Overlayed chromatograms for rat plasma, blank LNC (50 nm), and LNC-plasma mixture incubated for 1 h at 37°C. Arrows indicate fraction 1 (F1) and fraction 2 (F2), which were used for further experiments.

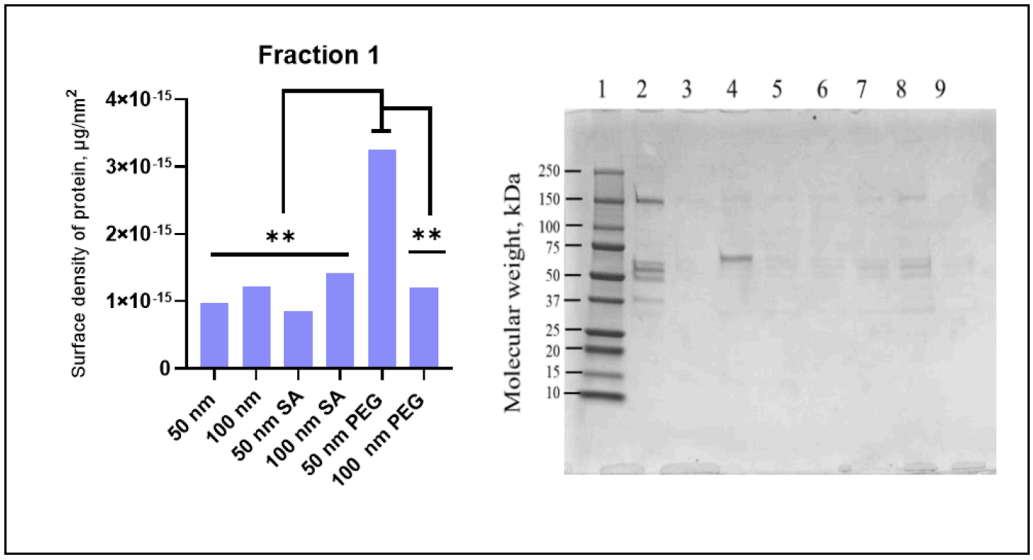

Fig. 6. **(A)** Protein quantity bound to different LNC formulations per unit of surface area (BCA assay). Data is expressed as mean ± standard deviation (measurement performed in duplicate). $^{**}p \leq 0.01$. **(B)** SDS-PAGE gel of LNC exposed to the protein of rat plasma, with framed sections representing the main intense bands (150 kDa, and 65 kDa) with black stars the higher bands level of intensity of the rat plasma exposed LNCs and red stars the higher bans level intensity of the rat plasma.

remaining bands represent the plasma proteins that bound to the LNCs during the incubation with rat plasma. The image of gel on Fig. 6B shows the results of the fraction 1 given after the SEC step. Two main bands probably correspond to albumin (65 kDa) and one other glycoprotein like a coagulation factor (150 kDa) (Palchetti et al., 2016). The most intense plasma protein bands (identified by black stars) correspond to the corona protein around LNC-50-PEG that seem in total accordance with the previous results of the protein quantification. These higher intensity bands (60 and 150 kDa) were also found on the rat plasma proteins profile. These results highlighted the fact that the main proteins present in the rat plasma had a high affinity for LNCs especially for LNC 50-PEG.

These results confirmed the NP evolution during plasmatic incubation. The LNC 50 nm with PEG addition has showed their higher diameter increasing due to protein adsorbed and thus a larger quantity of protein on their surface. As previously discussed, understanding PEG conformation on the NPs surface can explain these results because that did not correspond to an usual pegylation process (Allen et al., 2002; Mare et al., 2018). Adding to that, we can also focus on the PEG surface density because the quantity of added PEG was equal between LNC 50 and 100 nm (Supplementary Table S1). That lead to a higher PEG density for the LNC 50 as compared to the LNC 100 which can decrease the roughness and increase the protein corona formation (Bilardo et al., 2022). Walkey et al. (2012), have demonstrated on the one hand that increasing PEG density may further reduce serum protein adsorption on gold NPs. On the other hand, when the PEG density was fixed, the decrease of NP size lead to an increase of the total protein adsorption (Walkey et al., 2012). Even if we ~~have~~ modified simultaneously size and surface density of PEG, it seemed clear that the protein quantity adsorbed was a consequence of the NPs surface curvature with steric interactions between neighbouring PEGs. Finally, this confirmed that adsorption of proteins was probably stronger when PEG chains had more freedom on lower curvature surface. These findings also confirm that increasing PEG density on smaller NP will enhance the protein adsorption. As previously described, PEG mushroom-like conformations could be less efficient than PEG brush-like ones for protein adsorption. To complete these results, the last step of this study consists in the application of the soft particle theory of Ohshima (Ohshima, 2009; Ohshima,

2001).

3.4.1. Electrokinetics analysis of LNCs, a link between corona protein and soft particles

To understand the previous results on the corona protein formation, an electrokinetic study was performed using the Ohshima method (Ohshima, 2009). The goal of this study was to characterize the available thickness at the NP interface where proteins could interact with the interfacial compounds (mainly of PEG hydroxystearate mixture) and thus assess the influence of the interfacial molecular conformation.

The Table 1 shows estimated values of pseudo-charge density (ZN) and the accessibility layer to ions or proteins (1/λ), with specific calculation models based on Ohshima method. After calculation, this method enable to find a concordance between theoretical and experimental values by determining the best ZN and 1/λ values. The different values were presented in Table 1 as a function of LNCs type. It was decided to exclude NPs with electropositive charge related to stearylamine present in LNC-50-SA and LNC-100- SA formulations because the probe Cl^- was not well validated to use for Ohshima's method.

The usual LNC 50 and 100 nm without specific coatings displayed a negative pseudo-charge density and a very low ion penetration accessibility layer. For LNCs with PEG addition, the results presented in Table 1 showed little negative pseudo-charge density and high ion penetration accessibility layer. The decrease of pseudo-charge density of LNCs with PEG was linked to the addition of PEG, which lead to a steric hindrance layer in contrast to classical LNC formulations. Proteins, with mainly negative charges, seemed more in interaction with LNC-50-PEG with lower apparent negatively pseudo-charge compared to LNC-50. The similar phenomenon was observed for LNC-100-PEG *versus* LNC-100. Adding to that, the ion penetration layer which was higher for LNC-50-PEG than other LNCs confirmed our previous obtained results (protein quantification) with higher adsorbed protein surface density (Fig. 6A) and an increased hydrodynamic diameter (Fig. 4A).

If we focus on the LNC50-PEG ion penetration accessible layer and proteins adsorption, the high attractiveness could be due to a brush-like conformation facilitating the protein penetration in contrast to a mushroom-like conformation for LNC-100-PEG. This difference of PEG surface conformation can be linked to PEG surface density and surface curvature difference between 50 to 100 nm. Like it was previously described, the protein adsorption seems to be the result of curvature-dependent differences in PEG-PEG steric interactions (Walkey et al., 2012). Even if PEG addition is not similar to usual PEG grafting (Allen et al., 2002; Mare et al., 2018), this finding seems to be slightly in contrast to main works on this topic in which an increase in the PEG density decreases, and does not enhance, protein adsorption (Gref et al., 2000; Partikel et al., 2019; Rampado et al., 2020). Nowadays, the stealthiness of NPs is a concept which is not totally controlled. Some works explored deeper the procedure for NPs coating, to understand influence of polymers conformation and surface density to achieve the optimal stealth effect (Coty et al., 2017; Li et al., 2019). PEG density seems to play a major role in the long-circulating NP characteristics (Rampado et al., 2020; Park, 2010; Zhou et al., 2018). Interestingly, we recently showed an increased blood clearance of those LNCs 50 nm PEG compared to the five other LNCs after intravenous administration in rat (Lebreton et al., 2022). This observation was assigned to an increased instability of the LNCs 50 nm PEG in blood as compared to the other ones (Lebreton et al., 2022). Thus, the new data from the present study reveal that the difference in the protein corona formation, specifically on the LNC 50 nm PEG, is associated with their increased blood instability and increased blood clearance observed *in vivo*. It is now well accepted that surface changes in corona formation of organic nanoparticles are strongly correlated to biological and pharmacological changes like cell uptake and internalization (Sánchez-Moreno et al., 2015), in depth pharmacokinetics studies are now needed to decipher the link between PEG density, corona formation, the stability in blood and blood clearance.

Table 1
Estimated parameters, with Ohshima's method, pseudo-charge density ZN (C/m3) and the accessibility layer 1/λ (nm), for different LNCs.

	ZN (C/m^3)	1/λ (nm)
LNC-50	−4958	0.8
LNC-100	−664.9	3.3
LNC-50-PEG	−17.3	98.9
LNC-100-PEG	−32.6	55.7

4. Conclusion

To sumit up, this study shows that the protein-nanoparticle corona formation can be studied by different methods. Whether it is with zeta potential and size or protein quantification and even Ohshima method, all obtained results confirm protein adsorption on LNCs. Another important result is linked to PEG addition during formulation showing that it does not necessarily lead to stealth nanoparticles. It seems obvious to distinguish per-formulation and post-insertion PEG addition. Our method of PEG addition in the starting mixture modified the accessible penetration layer for proteins. Even if many studies have tried to find the best PEG density and conformation to guarantee a good stealthiness, it is now sure that proteins always manage to penetrate and adsorb on NPs surface. The current challenge is to improve characterization methods to assess the consequence of PEG density and length chain on protein corona formation. Moreover, our study confirms that a basic understanding of physicochemical properties of NP which impact the adsorption of protein is decisive for designing and developing nanomedicines. Knowing that, NPs characteristics in blood circulation (and trying to reach its targets) can be very different to their initial formulation because of protein corona formation. In the future, a deep understanding of the *in vivo* fate of NPs after intravenous administration with protein adsorption phenomenon is the first step to improve clinical translation.

Funding

This work was supported by Ligue contre le cancer Maine et Loire et Loiret Comitee (JPB/FP −441/12.2019 NANOPK PROJECT). Anastasiia Vasylaki was funded by NANOMED EMJMD supported by the European Union and the Erasmus+ Program by the European Union in the Framework Agreement Number 2016–2057/001–001 EMJMD, No. 574,439-EPP-1-FR-EPPKA1-JMD-MOB.

CRediT authorship contribution statement

Vincent Lebreton: Conceptualization, Methodology, Data curation, Visualization, Investigation, Writing – original draft. **Samuel Legeay:** Supervision, Writing – review & editing. **Anastasiia Vasylaki:** Investigation, Data curation, Methodology, Writing – original draft. **Frederic Lagarce:** Writing – review & editing. **Patrick Saulnier:** Conceptualization, Supervision, Validation, Writing – review & editing.

Declaration of Competing Interest

The authors declare that they have no known competing financial interests or personal relationships that could have appeared to influence the work reported in this paper.

Data availability

Data will be made available on request.

Acknowledgment

The authors would like to thank to Erwan AUTRET, for his proof-reading of English writing.

Supplementary materials

Supplementary material associated with this article can be found, in the online version, at doi:10.1016/j.ejps.2023.106537.

References

Allen, T.M., Sapra, P., Moase, E., 2002. Use of the post-insertion method for the formation of ligand-coupled liposomes. Cell. Mol. Biol. Lett. 7 (3), 889–894.
Berrecoso, G., Crecente-Campo, J., Alonso, M.J., 2020. Unveiling the pitfalls of the protein corona of polymeric drug nanocarriers. Drug Deliv. Transl. Res. 10, 730–750. https://doi.org/10.1007/s13346-020-00745-0.
Bertrand, N., Grenier, P., Mahmoudi, M., Lima, E.M., Appel, E.A., Dormont, F., Lim, J.M., Karnik, R., Langer, R., Farokhzad, O.C., 2017. Mechanistic understanding of *in vivo* protein corona formation on polymeric nanoparticles and impact on pharmacokinetics. Nat. Commun. 8 https://doi.org/10.1038/s41467-017-00600-w.
Bilardo, R., Traldi, F., Vdovchenko, A., Resmini, M., 2022. Influence of surface chemistry and morphology of nanoparticles on protein corona formation. WIREs Nanomed. Nanobiotechnol. 14 https://doi.org/10.1002/wnan.1788.
Caracciolo, G., 2015. Liposome-protein corona in a physiological environment: challenges and opportunities for targeted delivery of nanomedicines. Nanomed. Nanotechnol. Biol. Med. 11, 543–557. https://doi.org/10.1016/j.nano.2014.11.003.
Cedervall, T., Lynch, I., Lindman, S., Berggard, T., Thulin, E., Nilsson, H., Dawson, K.A., Linse, S., 2007. Understanding the nanoparticle-protein corona using methods to quantify exchange rates and affinities of proteins for nanoparticles. Proc. Natl. Acad. Sci. 104, 2050–2055. https://doi.org/10.1073/pnas.0608582104.
Cieślak, A., Wauthoz, N., Nieto Orellana, A., Lautram, N., Béjaud, J., Hureaux, J., Lafleur, M., Benoit, J.P., Salomon, C.J., Bastiat, G., 2017. Stealth nanocarriers based sterosomes using PEG post-insertion process. Eur. J. Pharm. Biopharm. https://doi.org/10.1016/j.ejpb.2017.02.008.
Coty, J.B., Oliveira, E.E., Vauthier, C., 2017. Tuning complement activation and pathway through controlled molecular architecture of dextran chains in nanoparticle corona. Int. J. Pharm. 532, 769–778. https://doi.org/10.1016/j.ijpharm.2017.04.048.
Demeester, J., Jiskoot, W., Crommelin, D., 2005. Methods For Structural Analysis of Protein Pharmaceuticals. AAPS, Arlington.
Fang, G., Zhang, Q., Pang, Y., Thu, H.E., Hussain, Z., 2019. Nanomedicines for improved targetability to inflamed synovium for treatment of rheumatoid arthritis: multi-functionalization as an emerging strategy to optimize therapeutic efficacy. J. Control. Release 303, 181–208. https://doi.org/10.1016/j.jconrel.2019.04.027.
Filipe, V., Hawe, A., Jiskoot, W., 2010. Critical evaluation of nanoparticle tracking analysis (NTA) by NanoSight for the measurement of nanoparticles and protein aggregates. Pharm. Res. 27, 796–810. https://doi.org/10.1007/s11095-010-0073-2.
Gazaille, C., Sicot, M., Akiki, M., Lautram, N., Dupont, A., Saulnier, P., Eyer, J., Bastiat, G., 2021. Characterization of biological material adsorption to the surface of nanoparticles without a prior separation step: a case study of glioblastoma-targeting peptide and lipid nanocapsules. Pharm. Res. 38 (4), 681–691. https://doi.org/10.1007/s11095-021-03034-8.
Gref, R., Luck, M., Quellec, P., Marchand, M., Dellacherie, E., Harnisch, S., Blunk, T., Muller, R.H., 2000. Stealth' corona-core nanoparticles surface modified by polyethylene glycol (PEG): influences of the corona (PEGchain length and surface density) and of the core composition on phagocytic uptake and plasma protein adsorption. Colloids Surf. B 301–313.
Groo, A.C., Bossiere, M., Trichard, L., Legras, P., Benoit, J.P., Lagarce, F., 2015. *In vivo* evaluation of paclitaxel-loaded lipid nanocapsules after intravenous and oral administration on resistant tumor. Nanomedicine 10, 589–601. https://doi.org/10.2217/nnm.14.124.
Gupta, M.N., Roy, I., 2020. How corona formation impacts nanomaterials as drug carriers. Mol. Pharm. 17, 725–737. https://doi.org/10.1021/acs.molpharmaceut.9b01111.
Gustafson, H.H., Holt-Casper, D., Grainger, D.W., Ghandehari, H., 2015. Nanoparticle uptake: the phagocyte problem. Nano Today. https://doi.org/10.1016/j.nantod.2015.06.006.
B. Heurtault, P. Saulnier, B. Pech, J.E. Proust, J.P. Benoit, A Novel Phase Inversion-Based Process For the Preparation of Lipid Nanocarriers, 2002.
Hierro-Oliva, M., Gallardo-Moreno, A.M., González-Martín, M.L., 2021. Surface characterisation of human serum albumin layers on activated ti6al4v. Materials 14. https://doi.org/10.3390/ma14237416 (Basel).
Hirsjärvi, S., Dufort, S., Gravier, J., Texier, I., Yan, Q., Bibette, J., Sancey, L., Josserand, V., Passirani, C., Benoit, J.P., Coll, J.L., 2013. Influence of size, surface coating and fine chemical composition on the *in vitro* reactivity and *in vivo* biodistribution of lipid nanocapsules *versus* lipid nanoemulsions in cancer models. Nanomed. Nanotechnol. Biol. Med. https://doi.org/10.1016/j.nano.2012.08.005.
Huynh, N.T., Passirani, C., Saulnier, P., Benoit, J.P., 2009. Lipid nanocapsules: a new platform for nanomedicine. Int. J. Pharm. https://doi.org/10.1016/j.ijpharm.2009.04.026.
Kari, O.K., Ndika, J., Parkkila, P., Louna, A., Lajunen, T., Puustinen, A., Viitala, T., Alenius, H., Urtti, A., 2020. *In situ* analysis of liposome hard and soft protein corona structure and composition in a single label-free workflow. Nanoscale 12, 1728–1741. https://doi.org/10.1039/c9nr08186k.
Ke, P.C., Lin, S., Parak, W.J., Davis, T.P., Caruso, F., 2017. A decade of the protein corona. ACS Nano 11, 11773–11776. https://doi.org/10.1021/acsnano.7b08008.
Kristensen, K., Engel, T.B., Stensballe, A., Simonsen, J.B., Andresen, T.L., 2019. The hard protein corona of stealth liposomes is sparse. J. Control. Release 307, 1–15. https://doi.org/10.1016/j.jconrel.2019.05.042.
Lebreton, V., Kaeokhamloed, N., Vasylaki, A., Hilairet, G., Mellinger, A., Béjaud, J., Saulnier, P., Lagarce, F., Gattacceca, F., Legeay, S., Roger, E., 2022. Pharmacokinetics of intact lipid nanocapsules using new quantitative FRET technique. J. Control. Release 351, 681–691. https://doi.org/10.1016/j.jconrel.2022.09.057.
Li, D., Wang, F., Di, H., Liu, X., Zhang, P., Zhou, W., Liu, D., 2019. Cross-linked poly (ethylene glycol) shells for nanoparticles: enhanced stealth effect and colloidal stability. Langmuir 35, 8799–8805. https://doi.org/10.1021/acs.langmuir.9b01325.
Lundqvist, M., Stigler, J., Elia, G., Lynch, I., Cedervall, T., Dawson, K.A., 2008. Nanoparticle size and surface properties determine the protein corona with possible implications for biological impacts. Proc. Natl. Acad. Sci. 105, 14265–14270. https://doi.org/10.1073/pnas.0805135105.
Lundqvist, M., Augustsson, C., Lilja, M., Lundkvist, K., Dahlbäck, B., Linse, S., Cedervall, T., 2017. The nanoparticle protein corona formed in human blood or human blood fractions. PLoS One 12. https://doi.org/10.1371/journal.pone.0175871.
I. Lynch, K.A. Dawson, Protein-nanoparticle interactions, 2008.
Lynch, I., Cedervall, T., Lundqvist, M., Cabaleiro-Lago, C., Linse, S., Dawson, K.A., 2007. The nanoparticle-protein complex as a biological entity; a complex fluids and surface science challenge for the 21st century. Adv. Colloid Interface Sci. 134–135, 167–174. https://doi.org/10.1016/j.cis.2007.04.021.
Machhi, J., Shahjin, F., Das, S., Patel, M., Abdelmoaty, M.M., Cohen, J.D., Singh, P.A., Baldi, A., Bajwa, N., Kumar, R., Vora, L.K., Patel, T.A., Oleynikov, M.D., Soni, D., Yeapuri, P., Mukadam, I., Chakraborty, R., Saksena, C.G., Herskovitz, J., Hasan, M., Oupicky, D., Das, S., Donnelly, R.F., Hettie, K.S., Chang, L., Gendelman, H.E., Kevadiya, B.D., 2021. Nanocarrier vaccines for SARS-CoV-2. Adv. Drug Deliv. Rev. https://doi.org/10.1016/j.addr.2021.01.002.
Mare, R., Paolino, D., Celia, C., Molinaro, R., Fresta, M., Cosco, D., 2018. Post-insertion parameters of PEG-derivatives in phosphocholine-liposomes. Int. J. Pharm. 552, 414–421. https://doi.org/10.1016/j.ijpharm.2018.10.028.
A. Mcgoron, M. Fujita, F. Jadidi-Niaragh, N.M. La-Beck, L.M. Wood, X. Liu, Harnessing Liposome Interactions With the Immune System For the Next Breakthrough in Cancer Drug Delivery, (2019). 10.3389/fphar.2019.00220.
Morille, M., Montier, T., Legras, P., Carmoy, N., Brodin, P., Pitard, B., Benoît, J.P., Passirani, C., 2010. Long-circulating DNA lipid nanocapsules as new vector for passive tumor targeting. Biomaterials. https://doi.org/10.1016/j.biomaterials.2009.09.044.
Mouzouvi, C.R.A., Umerska, A., Bigot, A.K., Saulnier, P., 2017. Surface active properties of lipid nanocapsules. PLoS One. https://doi.org/10.1371/journal.pone.0179211.
Nanomedicine and the COVID-19 vaccines. Nat. Nanotechnol., 2020. https://doi.org/10.1038/s41565-020-00820-0.
Ohshima, H., 2001. Dynamic electrophoretic mobility of a soft particle. J. Colloid Interface Sci. 233, 142–152. https://doi.org/10.1006/jcis.2000.7264.
Ohshima, H., 2006. Theory of Colloid and Interfacial Electric Phenomena, 1st ed. Academic Press.
Ohshima, H., 2009. Theory of electrostatics and electrokinetics of soft particles. Sci. Technol. Adv. Mater. 10 https://doi.org/10.1088/1468-6996/10/6/063001.
Palchetti, S., Colapicchioni, V., Digiacomo, L., Caracciolo, G., Pozzi, D., Capriotti, A.L., La Barbera, G., Laganà, A., 2016. The protein corona of circulating PEGylated liposomes. Biochim. Biophys. Acta Biomembr. 1858, 189–196. https://doi.org/10.1016/j.bbamem.2015.11.012.
Pareek, V., Bhargava, A., Bhanot, V., Gupta, R., Jain, N., Panwar, J., 2018. Formation and characterization of protein corona around nanoparticles: a review. J. Nanosci. Nanotechnol. 18, 6653–6670. https://doi.org/10.1166/jnn.2018.15766.
Park, K., Otte, A., Park, H., 2022. Perspective on drug delivery in 2050. J. Control. Release. https://doi.org/10.1016/j.jconrel.2022.02.025.
Park, K., 2010. To PEGylate or not to PEGylate, that is not the question. J. Control. Release 142, 147–148. https://doi.org/10.1016/j.jconrel.2010.01.025.
Park, S.J., 2020. Protein–nanoparticle interaction: corona formation and conformational changes in proteins on nanoparticles. Int. J. Nanomed. 15, 5783–5802. https://doi.org/10.2147/IJN.S254808.
Partikel, K., Korte, R., Stein, N.C., Mulac, D., Herrmann, F.C., Humpf, H.U., Langer, K., 2019. Effect of nanoparticle size and PEGylation on the protein corona of PLGA nanoparticles. Eur. J. Pharm. Biopharm. 141, 70–80. https://doi.org/10.1016/j.ejpb.2019.05.006.
Pelaz, B., Del Pino, P., Maffre, P., Hartmann, R., Gallego, M., Rivera-Fernández, S., De La Fuente, J.M., Nienhaus, G.U., Parak, W.J., 2015. Surface functionalization of nanoparticles with polyethylene glycol: effects on protein adsorption and cellular uptake. ACS Nano 9, 6996–7008. https://doi.org/10.1021/acsnano.5b01326.
Peltier, S., Oger, J.M., Lagarce, F., Couet, W., Benoît, J.P., 2006. Enhanced oral paclitaxel bioavailability after administration of paclitaxel-loaded lipid nanocapsules. Pharm. Res. 23, 1243–1250. https://doi.org/10.1007/s11095-006-0022-2.
Perrier, T., Saulnier, P., Benoît, J.P., 2010. Methods for the functionalisation of nanoparticles: new insights and perspectives. Chem. A Eur. J. https://doi.org/10.1002/chem.201000808.
Rampado, R., Crotti, S., Caliceti, P., Pucciarelli, S., Agostini, M., 2020. Recent advances in understanding the protein corona of nanoparticles and in the formulation of "Stealthy" nanomaterials. Front. Bioeng. Biotechnol. 8 https://doi.org/10.3389/fbioe.2020.00166.

Roger, E., Lagarce, F., Benoit, J.P., 2011. Development and characterization of a novel lipid nanocapsule formulation of Sn38 for oral administration. Eur. J. Pharm. Biopharm. https://doi.org/10.1016/j.ejpb.2011.01.021.

Saliou, B., Thomas, O., Lautram, N., Clavreul, A., Hureaux, J., Urban, T., Benoit, J.P., Lagarce, F., 2013. Development and *in vitro* evaluation of a novel lipid nanocapsule formulation of etoposide. Eur. J. Pharm. Sci. 50, 172–180. https://doi.org/10.1016/j.ejps.2013.06.013.

Sánchez-Moreno, P., Buzón, P., Boulaiz, H., Peula-García, J.M., Ortega-Vinuesa, J.L., Luque, I., Salvati, A., Marchal, J.A., 2015. Balancing the effect of corona on therapeutic efficacy and macrophage uptake of lipid nanocapsules. Biomaterials 61, 266–278. https://doi.org/10.1016/j.biomaterials.2015.04.049.

Sharifi, S., Caracciolo, G., Mahmoudi, M., 2020. Biomolecular corona affects controlled release of drug payloads from nanocarriers. Trends Pharmacol. Sci. 41, 641–652. https://doi.org/10.1016/j.tips.2020.06.011.

Tenzer, S., Docter, D., Rosfa, S., Wlodarski, A., Kuharev, J., Rekik, A., Knauer, S.K., Bantz, C., Nawroth, T., Bier, C., Sirirattanapan, J., Mann, W., Treuel, L., Zellner, R., Maskos, M., Schild, H., Stauber, R.H., 2011. Nanoparticle size is a critical physicochemical determinant of the human blood plasma corona: a comprehensive quantitative proteomic analysis. ACS Nano 5, 7155–7167. https://doi.org/10.1021/nn201950e.

Tran, S., DeGiovanni, P.J., Piel, B., Rai, P., 2017. Cancer nanomedicine: a review of recent success in drug delivery. Clin. Transl. Med. https://doi.org/10.1186/s40169-017-0175-0.

Treuel, L., Docter, D., Maskos, M., Stauber, R.H., 2015. Protein corona - from molecular adsorption to physiological complexity. Beilstein J. Nanotechnol. 6, 857–873. https://doi.org/10.3762/bjnano.6.88.

D.A. Tyrrell, V.J. Richardson, B.E. Ryman, The effect of serum protein fractions on liposome-cell interactions in cultured cells and the perfused rat liver, 1977.

Vilanova, O., Mittag, J.J., Kelly, P.M., Milani, S., Dawson, K.A., Rädler, J.O., Franzese, G., 2016. Understanding the kinetics of protein-nanoparticle corona formation. ACS Nano 10, 10842–10850. https://doi.org/10.1021/acsnano.6b04858.

Walkey, C.D., Olsen, J.B., Guo, H., Emili, A., Chan, W.C.W., 2012. Nanoparticle size and surface chemistry determine serum protein adsorption and macrophage uptake. J. Am. Chem. Soc. 134, 2139–2147. https://doi.org/10.1021/ja2084338.

Zhou, H., Fan, Z., Li, P.Y., Deng, J., Arhontoulis, D.C., Li, C.Y., Bowne, W.B., Cheng, H., 2018. Dense and dynamic polyethylene glycol shells cloak nanoparticles from uptake by liver endothelial cells for long blood circulation. ACS Nano. 12 (10), 10130–10141. https://doi.org/10.1021/acsnano.8b04947.